Evolution of Ate- organoiron(II) species towards lower oxidation states: role of the steric and electronic factors

Lidie Rousseau, Christian Herrero, Martin Clémancey, Arnaud Imberdis, Geneviéve Blondin, Guillaume Lefèvre

Evolution of *ate* organoiron(II) species towards lower oxidation states: role of the steric and electronic factors

Lidie Rousseau[b], Christian Herrero[c], Martin Clémancey[d], Arnaud Imberdis[b], Geneviève Blondin*[d] and Guillaume Lefèvre*[a,b]

Abstract: *Ate*-iron(II) species such as $[Ar_3Fe^{II}]^-$ (Ar = aryl) are key intermediates in Fe-catalyzed cross-coupling reactions between aryl nucleophiles and organic electrophiles. They can be active species in the catalytic cycle, or lead to Fe^0 and Fe^I oxidation states, which can themselves be catalytically active or lead to unwished organic byproducts. Analysis of the reactivity of the intermediates obtained by step-by-step displacement of the mesityl groups in high-spin $[Mes_3Fe^{II}]^-$ by less hindered phenyl ligands was performed, and enlightened the crucial role of both steric and electronic parameters in the formation of the Fe^0 and Fe^I oxidation states. The formation of quaternized $[Ar_4Fe^{II}MgBr(THF)]^-$ intermediates allows to reduce the bielectronic reductive elimination energy required for the formation of Fe^0. Similarly, a small steric pressure of the aryl groups in $[Ar_3Fe^{II}]^-$ enables the formation of dimeric aryl-bridged $[\{Fe^{II}(Ar)_2\}_2(\mu\text{-}Ar)_2]^{2-}$ species, which afford the Fe^I oxidation state by bimetallic reductive elimination. These results are supported by ^1H NMR, EPR and ^{57}Fe-Mössbauer spectroscopies, as well as by DFT calculations.

Introduction

Achieving efficient C–C bond formation by iron-catalyzed cross-coupling between a nucleophilic partner and an organic electrophile represents an interesting alternative to palladium catalysis, due to iron cheap cost and eco-compatibility.[1] The first efficient Fe-mediated cross coupling methodologies between Grignard reagents and organic electrophiles were discovered by Kochi in the 1970s[1a-b] and considerably extended thanks to the pioneer work of Cahiez,[1c] followed by Fürstner[1d] and Bedford.[1e] This field is still gaining interest since the nature of the elementary steps involving transitory iron intermediates continues to arise mechanistic debates. Some of the mechanisms at play in these transformations have just been recently unveiled, mostly thanks to the use of physical-inorganic techniques such as Mössbauer and EPR spectroscopies, and magnetic circular dichroism (MCD).[1e-j] These techniques demonstrated recently that numerous Fe-catalyzed cross-coupling reactions between main-group organometallics and alkyl electrophiles involved the formation of transient organoiron(II) intermediates as key reactive species (Scheme 1a). Diphosphine-ligated monoaryliron(II) species (P,P)Fe^{II}(Ph)(X) proved to be extremely reactive in C_{sp2}–C_{sp3} bond formation.[2a] Similarly, mono- and bis-alkynyliron(II) diphosphine-stabilized species were found to be kinetically competent to ensure alkynyl-alkyl cross-coupling.[2b] Bedford demonstrated that anionic *ate*-Fe^{II} adducts such as $[Mes_3Fe^{II}]^-$ and $[(PhCH_2)_3Fe^{II}]^-$ were also able to catalyze C_{sp2}–C_{sp3} and C_{sp3}–C_{sp3} cross-couplings.[3] Neidig recently reported that N-Heterocyclic-Carbene-stabilized (NHCs) bis-alkyliron(II) species such as (IMes)Fe^{II}((1,3-dioxan-2-yl)ethyl)$_2$) are highly efficient in C_{sp3}–C_{sp3} cross-coupling, unveiling the importance of the presence of ligating groups onto the Grignard alkyl chains in the stabilization of the active Fe^{II} catalyst.[4]

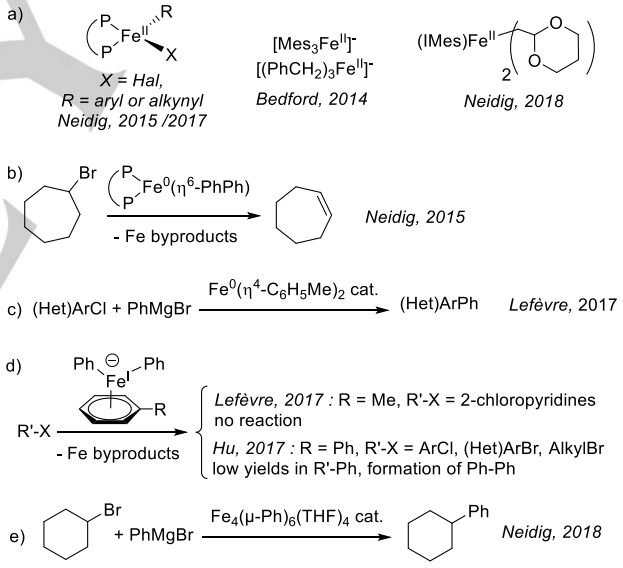

Scheme 1. a) Selected examples of Fe^{II} complexes active in C–C cross-coupling with alkyl electrophiles; b) Fe^0 species acting as off-cycle or c) catalytically-active intermediates in several couplings; d) examples of off-cycle Fe^I species; e) cross-coupling system catalyzed by a tetranuclear cluster featuring two Fe^I centers. (P,P) = C_6H_4-1,2-(P(C_6H_3-3,5-tBu_2)$_2$)$_2$; Mes = 2,4,6-$C_6H_2Me_3$; IMes = 1,3-bis(2,4,6-trimethylphenyl)-imidazolium.

These results attest to the catalytic activity of organoiron(II) species in several Fe-mediated cross-coupling systems, especially those involving alkyl electrophiles. They also reveal in those cases that formation of oxidation states lower than +II was not a prerequisite to ensure efficient cross-coupling processes.[5] Lower oxidation states such as Fe^0 and Fe^I are formed by *in situ* reduction of the iron precatalyst, and were often evidenced in

[a] Dr G. Lefèvre
Chimie ParisTech, PSL University, CNRS, Institute of Chemistry for Life and Health Sciences, CSB2D, 75005 Paris, France.
E-mail: guillaume.lefevre@chimieparistech.psl.eu
[b] Dr G. Lefèvre, L. Rousseau, A. Imberdis
NIMBE, CEA, CNRS, Univ. Paris-Saclay, 91191 Gif, France
[c] Dr C. Herrero
Institut de Chimie Moléculaire et des matériaux d'Orsay (UMR 8182)
Univ Paris Sud, Université Paris Saclay. 91405 Orsay cedex, France
[d] Dr M. Clémancey, Dr G. Blondin,
Univ. Grenoble Alpes, CNRS, CEA, LCBM (UMR 5249), pmb, 38000 Grenoble, France

various catalytic systems involving exogenous ligands (e.g. diphosphines[6a] or NHCs[6b]) or in co-ligand-free conditions.[6c] The reactivity of these low oxidation states is however very versatile. For example, Neidig demonstrated that (P,P)Fe^0(η^6-PhPh), formed from aryl-iron(II) species such as (P,P)$Fe^{II}(Ph)_2$, was not kinetically active towards alkyl electrophiles in cross-coupling conditions. Quite the opposite, this Fe^0 complex leads to the destruction of the alkyl electrophile by a parasitic β–elimination reaction (Scheme 1b).[2a] On the other hand, some of us demonstrated that the bis-arene-coordinated species (η^4-$C_6H_5Me)_2Fe^0$ could efficiently catalyze the cross-coupling between heteroaryl chlorides and aryl Grignard reagents (Scheme 1c).[7] Similarly, some Fe^I mononuclear species proved to be catalytically non-reactive in aryl-(hetero)aryl and aryl-alkyl Kumada cross-coupling (as it is the case for [(η^6-arene)$Fe^I(Ph)_2]^-$, arene = C_6H_5Me or PhPh, Scheme 1d [7,8]), whereas the tetranuclear cluster [$Fe_4(\mu$-$Ph)_6(THF)_4$], which formally contains two Fe^I centers, was found to be an excellent catalyst for aryl-alkyl cross-coupling (Scheme 1e).[9]

There is therefore no single unified mechanistic picture of the iron-catalyzed C–C bond formation between a main-group nucleophile and an organic electrophile, since the nature of the active oxidation state strongly depends on the nature of the reagents involved. The development of new and efficient Femediated cross-couplings therefore requires new frameworks enabling a fine control of the iron species distribution, giving the possibility to inhibit the formation of unwanted oxidation states. So far, the formation of Fe^0 and Fe^I species in cross-coupling mediums can be hardly controlled. A deep understanding of the formation mechanism of these oxidation states is thus fundamental if one wants to finely monitor their presence in the reaction medium. However, in-depth mechanistic investigations of the low oxidation states formation from polyhydrocarbyl-Fe^{II} species is scarce. In particular, stereoelectronic parameters governing these transformations are generally overlooked.

To investigate more closely the role of the hydrocarbyl ligands in the evolution of organoiron(II) intermediates towards lower oxidation states, we took inspiration from the difference observed between coordinated mesityl and phenyl iron complexes. It has been previously noticed that whereas several bis-mesitylated iron(II)-bisphosphine complexes have been isolated,[10,11] no bis-phenyl analogous complexes have been reported.[2a] Along this line, the two ferrous complexes with mesityl groups as unique ligands, namely [$Mes_3Fe^{II}]^-$ and [$Mes_4Fe^{II}_2$], have been characterized by X-ray diffraction several years ago.[12-14] This contrasts with the recent X-ray structure of [{$Fe^{II}(Ph)_2$}$_2$(μ-$Ph)_2]^{2-}$, trapped at –80°C,[9] to the best of our knowledge the unique ferrous complex with phenyl ligands only. In this work, we present the action of phenylmagnesium bromide on the kinetically stable species [$Mes_3Fe^{II}]^-$ and demonstrate, relying on ^{1}H NMR, EPR and Mössbauer spectrosocopies, that the mesityl ligands are successively substituted by phenyl groups, generating sterically less hindered ferrous complexes that further evolved toward Fe^0 and Fe^I species. The use of [$Mes_3Fe^{II}]^-$ as a starting material to reach phenylated intermediates allowed to investigate closely the role of steric effects in the evolution of the latter species. DFT calculations were performed to decipher the differences of reactivity between mesityl and phenyl ligands.

Results and Discussion

Substitution of the mesityl ligands in [$Mes_3Fe^{II}]^-$ by phenyl groups

Figure 1a reproduces the ^{1}H NMR spectrum recorded after the addition of 4 equiv. of MesMgBr on $FeCl_2$ in THF. This spectrum is similar to those previously reported for the mononuclear-complex [$Mes_3Fe^{II}]^-$.[3,10] According to the relative intensities and to the similarities in positions and linewidths of the mesityl resonances in the high-spin S = 2 [$py_2Fe^{II}Mes_2$] complex,[11] the three signals detected at 22, 115 and 131 ppm can be attributed to the two *ortho*-CH_3 (18H), the unique *para*-CH_3 (9H) and the two *meta*-H (6H), respectively. There is no evidence for neither the formation of the dinuclear [$Mes_4Fe^{II}_2$] complex that presents in deuterated benzene a spectrum restricted to the 25 to -7 ppm window[13] owing the strong antiferromagnetic interaction between the two high-spin Fe^{II} ions,[15] nor the solvated mononuclear fragment Mes_2Fe^{II} expected to be generated by dissociation of [$Mes_4Fe^{II}_2$] in THF (60 (12H, *ortho*-CH_3), 83 (6H, *para*-CH_3), and 110 (4H, *meta*-H) ppm).[13] Moreover, [$Mes_3Fe^{II}]^-$ remains stable in solution because no alteration of the ^{1}H NMR spectrum is observed after 12h.[16]

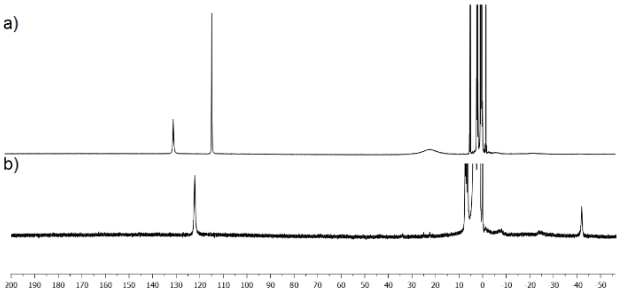

Figure 1. ^{1}H NMR spectrum of a) [$Mes_3Fe^{II}]^-$ (T = 20°C); b) $FeCl_2$ + 3.4 equiv. PhMgBr (T = -30°C; no signal was observed in the 200-280 ppm area).

The stability of the [$Mes_3Fe^{II}]^-$ complex solution contrasts with that observed when 3.4 equiv. of PhMgBr are added to $FeCl_2$ in THF. Figure 1b reproduces the ^{1}H NMR spectrum recorded at -30°C, upon the regular increase of the temperature from -78 to 0°C (see Figure S1). Two transitory sharp paramagnetically shifted singlets, the first one lying between -50 and -35 ppm, the second between 110 and 155 ppm, are detected. These signals, in a close to 1:2 ratio, are tentatively attributed to the high-spin (S = 2) [$Ph_3Fe^{II}]^-$ complex. They collapsed in the 0-10°C range, which is consistent with the 50 s lifetime estimated by ESI-MS spectroscopy for this complex.[17] We can reasonably hypothesize that the signals at -42 and 122 ppm (T = -30°C, see Figure 1b) correspond to the *para*- (3H) and the two *meta*-H (6H) of the phenyl rings, the signal of the two *ortho*-H being too

broadened to be observed because of their proximity with the paramagnetic Fe^{II} ion.

With these characterizations in hands, treatment by increasing equivalents of PhMgBr of a $[Mes_3Fe^{II}]^-$ solution, prepared by the addition of 4 equiv of MesMgBr on $FeCl_2$ in THF, was investigated. ^{1}H NMR spectra displayed in Figure 2a demonstrate that addition of 1 to 5 equiv. of PhMgBr leads to the formation of two new paramagnetic species (**1** and **2**) exhibiting sharp singlets in the 90/140 ppm and in the -45/-40 ppm zones. Species **1** is characterized by signals at 132, 118, 100 and -42 ppm that are approximately in a 4:6:2:1 ratio and species **2** by signals at 133, 119, 101 and –40 ppm in a close to 2:3:4:2 ratio. Comparison with the ^{1}H NMR signatures of $[Mes_3Fe^{II}]^-$ and $[Ph_3Fe^{II}]^-$ suggests that the 132/133 and 118/119 ppm signals originate from the *meta*-H and *para*-CH_3 of mesityl ligands and that those at 100/101 and -42/-40 ppm correspond to the *meta*-H and *para*-H of coordinated phenyl rings in high-spin Fe^{II} mononuclear complexes. Moreover, based on the variations in intensity of the 130-135 ppm signals, the total quantity of $[Mes_3Fe^{II}]^-$ decreases during the process, whereas the quantity of **1** progressively increases upon the addition of 1-3 equiv. of PhMgBr, before decreasing for higher PhMgBr quantities. Concomitantly the quantity of **2** slightly increases (Figure 2b).

All these observations converge to identify 1 and 2 as the high-spin mixed-aryl *ate* $[Mes_2PhFe^{II}]^-$ and $[MesPh_2Fe^{II}]^-$ complexes, respectively. We can't exclude the formation of the three substituted complex $[Ph_3Fe^{II}]^-$ that wouldn't be detected owing its high instability. Generation of 1 and 2 is further supported by the GS-MS analyses (see Figure 2c). Whereas Mes–Mes is the only biaryl identified when analyzing the starting $[Mes_3Fe^{II}]^-$ solution, the addition of increasing amounts of PhMgBr led also to the detection of the mixed Mes–Ph biaryl along with Ph–Ph. It is well-established that the acidic quench of *ate* Fe^{II} species performed for this analysis can lead to the formation of biaryl compounds due to the decomposition of the iron complexes.[2a] However, the detection of Mes–Ph and Ph–Ph is a strong indication of mixed Mes/Ph and bis-phenyl Fe^{II} coordination spheres.

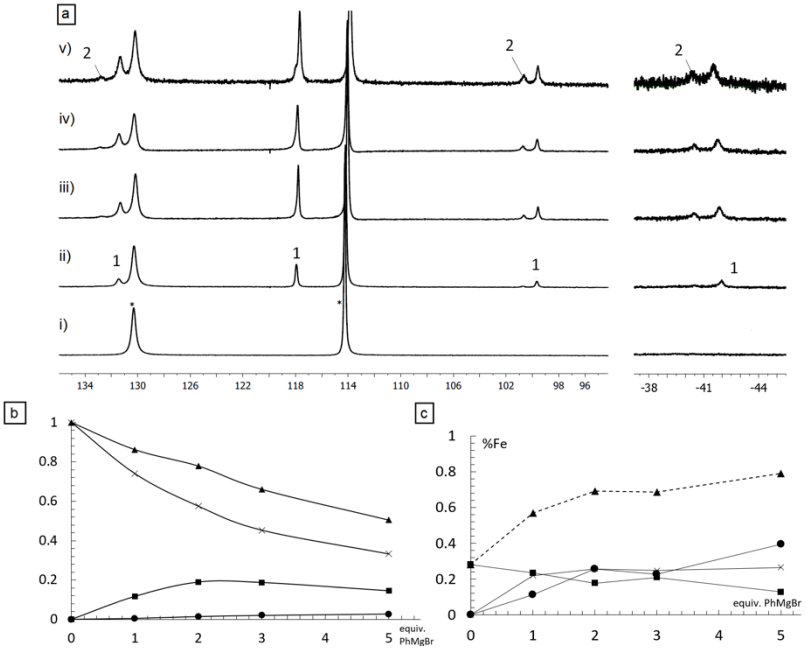

Figure 2. a) ^{1}H NMR downfield and upfield zones (resp. vertical scales: 1:1 and 1:3) of a solution of $[Mes_3Fe^{II}]^-$ (starred peaks) treated by increasing amounts of PhMgBr (i-v: 0, 1, 2, 3, 5 equiv. PhMgBr, T = 20°C; reaction time: 4 min); b) ^{1}H NMR quantification of the $[Mes_3Fe^{II}]^-$ (x), **1** (■), **2** (●) ratios *vs* internal standard (TMS_2O) in the spectra displayed Figure 2a, as a function of the PhMgBr quantity ($[Mes_3Fe^{II}]^-$ + **1** + **2** *vs* TMS_2O:▲); c) GC-MS quantification of Mes–Mes (■), Mes–Ph (x) and Ph–Ph (●) (sum: ▲), obtained upon treatment of a solution of $[Mes_3Fe^{II}]^-$ with 0-5 equiv. PhMgBr, after 4 minutes at 20°C.

Formation of reduced iron species

^{1}H NMR monitoring of the action of PhMgBr on $[Mes_3Fe^{II}]^-$ evidenced that the total amount of high-spin Fe^{II} mononuclear complexes decreases upon increasing equivalents of added PhMgBr (Figure 2b). Approximately 15 and 20% of iron species with no ^{1}H NMR signature are formed upon the addition of 1 and 2 equiv. of PhMgBr, respectively. This strongly suggests that the mixed Mes/Ph species $[Mes_2PhFe^{II}]^-$ and $[MesPh_2Fe^{II}]^-$ (as well as the putative $[Ph_3Fe^{II}]^-$), formed by substitution of the mesityl ligands of $[Mes_3Fe^{II}]^-$ by phenyls, are unstable at room temperature and lead to NMR-silent species within the time frame of the experiments (4 min at 20°C herein, Figure 2a). This hypothesis was confirmed when the addition of 1 equiv. PhMgBr onto $[Mes_3Fe^{II}]^-$ was monitored at -40°C (see Figure S2, top). At this temperature, 100% of the iron quantity remains in solution as NMR-detected *ate*-Fe^{II} species. A distribution of $[Mes_3Fe^{II}]^-$ (75% of the overall iron quantity), $[Mes_2PhFe^{II}]^-$ (21%), $[MesPh_2Fe^{II}]^-$ (3%) and $[Ph_3Fe^{II}]^-$ (1%) was observed, and remained unchanged after 2 hours at -40°C. At 20°C, the three later species, $[Mes_2PhFe^{II}]^-$, $[MesPh_2Fe^{II}]^-$, and $[Ph_3Fe^{II}]^-$, are prompt to undergo decomposition, since they respectively represent only 12%, 1% and 0% of the overall iron quantity after 4 minutes at this temperature, whereas the amount of $[Mes_3Fe^{II}]^-$ is unchanged (ca. 75%, see Figure 2a-ii). Further shift of the Mes/Ph exchange towards the formation of phenylated species and decomposition of the latter is observed at 20°C with increased reaction times, and the following distribution is observed by ^{1}H NMR after 30 minutes : $[Mes_3Fe^{II}]^-$ (57% of the overall iron quantity), $[Mes_2PhFe^{II}]^-$ (12%), $[MesPh_2Fe^{II}]^-$ (<2%) (Figure S2, bottom). 29% of the Fe containing species are thus NMR-silent after 30 minutes at 20°C. This led us to investigate the iron distribution obtained after decomposition of the *ate*-Fe^{II} complexes by means of EPR and Mössbauer spectroscopies.

Figure 3a reproduces the X-band EPR spectra recorded at 60 K after the addition of 1 and 2 equiv. of PhMgBr on in situ prepared $[Mes_3Fe^{II}]^-$ complex in THF:Toluene mixture. Weak signals in the g = 2 region and below 100 mT are detected that can be assigned to S = 1/2 and S = 5/2 species, respectively. Those signals are enhanced upon the addition of greater excess of PhMgBr (see Figures S3-4). The signal observed

between 300 and 350 mT presents the same *g*-values (2.20, 2.02 and 2.00) than the species previously detected after addition of 30 equiv. of PhMgBr on $FeCl_2$ and assigned to the low-spin complex $[(\eta^6\text{-}C_6H_5Me)Fe^{I}Ph_2]^-$.[7] This suggests that the same species can be formed albeit starting from a different Fe^{II} source. Quantification of the EPR signals (see Figure S5) indicates that less than 1% of iron is reduced to the +I state and oxidized to the +III state if less than 2 equiv. of PhMgBr are added (ca. 5% of Fe^{I} species being generated upon addition of 30 equiv. PhMgBr). These ratios did not significantly evolve after 30 minutes at 20°C. In a second time, a THF solution of in situ prepared $[Mes_3Fe^{II}]^-$ was treated by 1 equiv. of PhMgBr and analyzed by Mössbauer spectroscopy after filtration and removal of the volatiles (overall reaction time: 30 minutes at 20°C, see Figure 3b).

The solid-state spectrum could be simulated with three quadrupole doublets. The corresponding simulation parameters for species I, II and III are given in Table 1 (entries 1-3).

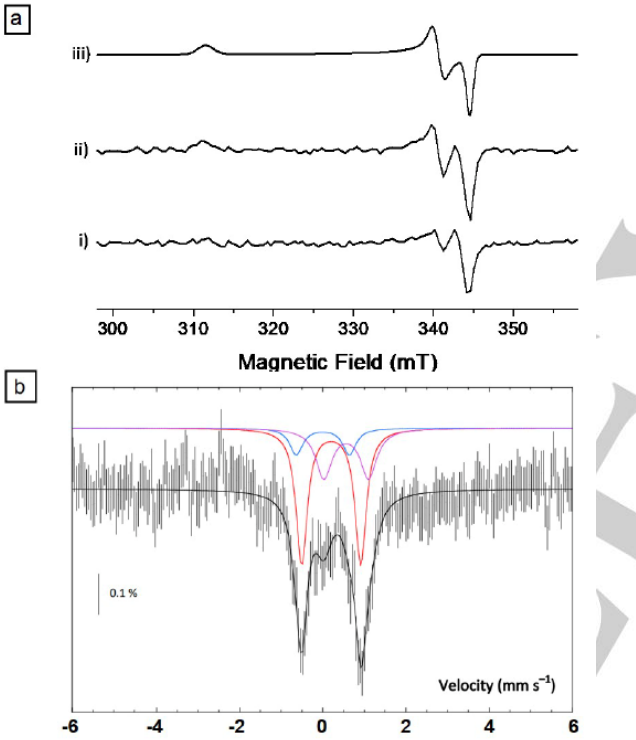

Figure 3. a) EPR analysis of a $[Mes_3Fe^{II}]^-$ solution in THF:toluene 1:10 mixture, treated by 1 (i) and 2 (ii) equiv. of PhMgBr. T = 60 K; samples frozen after 4 minutes at 20°C, *g* = 2 area (low-spin Fe^{I} resonances – see SI for high-spin Fe^{III} area); (iii): simulation of spectrum (ii) (simulation parameters: see SI); b) solid-state Mössbauer spectrum of a solution of $[Mes_3Fe^{II}]^-$ treated with 1 equiv. PhMgBr in THF after filtration and removal of the volatiles (overall reaction time : 30 minutes at 20°C, natural ^{57}Fe abundance, spectrum recorded at 80 K in the absence of external magnetic field).

The nuclear parameters of the species I and II are relevant of high-spin (*S* = 2) Fe^{II} species. The more intense doublet, accounting for 57% of the total iron content, can be attributed to $[Mes_3Fe^{II}]^-$ (δ_I = 0.20 mm.s^{-1}, $\Delta E_{Q,I}$ = 1.42 mm.s^{-1}, red line, Figure 3b, and Table 1, entry 1; see also Figure S6 for the comparison with the Mössbauer spectrum of an authentic sample). The relative amount of $[Mes_3Fe^{II}]^-$ is in agreement with what was detected by ^{1}H NMR spectroscopy in identical conditions ($[Mes_3Fe^{II}]^-$ treated by 1 equiv. PhMgBr after 30 minutes at 20°C, vide supra), since 57% of $[Mes_3Fe^{II}]^-$ were also detected in solution by this technique. The species II, accounting for ca. 13% of the iron quantity according to Mössbauer speciation (blue line, Figure 3b, and Table 1, entry 2), also echoes the ^{1}H NMR observations where 12% of $[Mes_2PhFe^{II}]^-$ is observed (Figure S2). The attribution of doublet II to this species is also sustained by DFT prediction of the isomer shift of $[Mes_2PhFe^{II}]^-$ (see SI and Table 1, entry 4), which proved to be smaller by ca. 0.2 mm.s^{-1} than isomer shift of $[Mes_3Fe^{II}]^-$, in line with the experimental Mössbauer spectrum (δ_{II} = 0.00 mm.s^{-1}, $\Delta E_{Q,II}$ = 1.28 mm.s^{-1}, Table 1). The possible presence of the dimeric species $[\{Fe^{II}(Mes)\}_2(\mu\text{-}Mes)_2]$ in this solid-state spectrum was ruled out by comparison with an authentic sample (δ = 0.39 mm.s^{-1}, ΔE_Q = 1.56 mm.s^{-1}, Figure S7). The third doublet with nuclear parameters δ_{III} = 0.56 mm.s^{-1}, $\Delta E_{Q,III}$ = 1.07 mm.s^{-1} (pink line) accounts for ca. 30% of the total iron content (Figure 3b and Table 1, entry 3). Since this quantity corresponds as well to the quantity of ^{1}H NMR-silent species obtained under the same conditions (Figure S2), this is likely that species III accounts for this fraction of iron.

The nuclear parameters of species III are reminiscent of those recently reported after the addition of 4 equiv. of PhMgBr on $FeCl_2$ in THF (δ = 0.50 mm.s^{-1}, ΔE_Q = 1.06 mm.s^{-1}).[18] This broad signal – the Lorentzian fullwidth at half-height is no lower than 0.90 mm.s^{-1} – was said to be indicative of at least one Fe^{III} species that would result from the decomposition of $[Ph_3Fe^{II}]^-$, as evidenced by ESI-MS. In the present case, EPR studies exclude the formation of such high quantity of *S* = 5/2 or *S* = 1/2 species (vide supra), suggesting that if Fe^{III} species are generated, they should be present as dinuclear complexes with a strong exchange interaction between the two Fe^{III} ions leading to EPR silent integer spin ground state species. That the +III oxidation state corresponds to the major part of iron in the solution investigated here is also disfavored according to the dinuclear $[\{Fe^{II}(Ph)_2\}_2(\mu\text{-}Ph)_2]^{2-}$ and tetranuclear $[Fe^{I,II}4(\mu\text{-}Ph)_6(THF)_4]$ complexes recently characterized upon the action of PhMgBr on a Fe^{III} source.[9] We have previously demonstrated that the addition of an even more important excess of PhMgBr on $FeCl_2$ in THF/Toluene mixture led to the formation of diamagnetic species accounting for 85% of the iron content, and identified as

Table 1. Distribution of the iron-containing species detected by ^{57}Fe-Mössbauer spectroscopy in spectrum displayed Figure 3c. δ, ΔE_Q and Γ in mm.s^{-1}; % av. error: 5%. [a] calculated values; av. error: ± 0.2 mm.s^{-1}.

Entry	Species	Fe ox. state	Spin	δ	ΔE_Q	Γ	%
1	I	Fe^{II}	2	0.20	1.42	0.32	57
2	II	Fe^{II}	2	0.00	1.28	0.38	13
3	III	Fe^{0}	0	0.56	1.07	0.47	30
4[a]	$[Mes_3Fe^{II}]^-$ $[Mes_2PhFe^{II}]^-$ $[MesPh_2Fe^{II}]^-$	Fe^{II}	2	0.04 -0.13 -0.12	-	-	-

the Fe^0 complex $[(\eta^4\text{-}C_6H_5Me)_2Fe^0]$.[7] Despite of the lack of toluene in the present study, we propose that species II corresponds to a diamagnetic Fe^0 complex. The lower amount detected in the present work is consistent with the lower added quantity of PhMgBr. This attribution is also sustained by the similar nuclear parameters determined at 77 K for the Fe^0 species $[(\eta^6\text{-}C_6H_6)Fe^0(\eta^4\text{-}C_6H_8)]$ (δ = 0.49 mm.s^{-1}, ΔE_Q = 0.92 mm.s^{-1}).[19] Moreover, detection of Fe^0 is in agreement with the formation of the biaryl compounds detected by GC-MS (see Figure 2c). It should be noticed that whereas 28% of Mes–Mes are detected on the starting solution, the addition of the first equivalent of PhMgBr led to the formation of a total amount of 57% of biaryl compounds, mainly Mes–Ph and Ph–Ph, corresponding to a doubling of the C–C coupling. Further additions of PhMgBr result in a much lower increase of biaryl molecules, 4–9% per equivalent of Grignard reactant. This behavior strongly suggests that biaryl compounds, namely Mes–Ph and Ph–Ph, are present prior the acidic quench of the reaction when PhMgBr is added. They would be formed by a 2-electron reductive elimination from Fe^{II} precursors that would concomitantly led to the release of Fe^0 species.

As demonstrated in this section, the reaction of $[Mes_3Fe^{II}]^-$ with an excess of PhMgBr leads to transient *ate*-Fe^{II} species $[Mes_2PhFe^{II}]^-$ and $[MesPh_2Fe^{II}]^-$, as well as to the thermally unstable $[Ph_3Fe^{II}]^-$ complex. These species exhibit a steric pressure around the Fe^{II} center less important than in $[Mes_3Fe^{II}]^-$,due to the substitution of mesityl by phenyl groups. Concomitantly, the formation of biaryl products is observed, as well as iron species with oxidation states lower than +II, the 0 being preponderantly generated. The following section is devoted to discuss the mechanistic features connecting those *ate* Fe^{II} intermediates with firstly Fe^0 and secondly Fe^I species in the presence of an excess of aryl Grignard reagent, with the help of DFT calculations.

Formation and reactivity of mixed Mes/Ph high-spin Fe^{II} complexes

The thermodynamic feasibility of the mesityl-phenyl ligand exchange connecting $[Mes_3Fe^{II}]^-$ to $[Mes_2PhFe^{II}]^-$, $[MesPh_2Fe^{II}]^-$ and putatively to $[Ph_3Fe^{II}]^-$ has been evaluated by DFT calculations (Scheme 2).

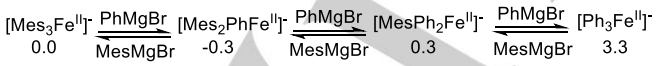

Scheme 2. Mesityl/Phenyl ligand exchange connecting the successive $[Mes_{3-n}Ph_nFe^{II}]^-$ species (n = 0-3) with DFT-computed energy (kcal.mol^{-1}) for each high-spin Fe^{II} complex (S = 2, quintuplet).

From a structural standpoint, phenyl rings in these aryl–Fe complexes tend to be less inclined with respect to the FeC_3 equatorial plane than the mesityls, due to the absence of sterically hindered methyl groups in ortho positions in the former (av. corresponding dihedral angles : 56° in $[Mes_3Fe^{II}]^-$ vs 30° in $[Ph_3Fe^{II}]^-$). All $[Mes_{3-n}Ph_nFe^{II}]^-$ species (n = 0-3) involved in these exchange reactions coexist within a narrow energetic span (3.3 kcal.mol^{-1}, Scheme 2), explaining why a progressive substitution of the mesityl ligands of $[Mes_3Fe^{II}]^-$ by phenyl anions can occur upon addition of increasing amounts of PhMgBr. This narrow energy distribution supports equilibria in solution and thus the coexistence of several *ate*-Fe^{II} species. We then sought for a mechanistic interpretation of this progressive Mes/Ph scrambling. The feasibility of the Mes/Ph ligand exchange connecting the $[Mes_{3-n}Ph_nFe^{II}]^-$ species by successive associative/dissociative mechanisms through quaternized Fe^{II} intermediates has been examined, inspired by the reactivity of iron salts with aryl lithium reagents. In the presence of strongly nucleophilic main-group organometallic reagents such as ArLi, it has already been reported that $FeCl_2$ and $FeCl_3$ can evolve towards quaternized *ate*-Fe^{II} complexes.[20] Pseudo-tetrahedral $[Ar_4Fe^{II}]^{2-}$ structures have been determined by X-ray diffraction in $[Np_4Fe][Li(OEt_2)]_2$[20a] and $[Ph_4Fe][Li(OEt_2)_2][Li(1,4\text{-dioxane})_2]$[20b] (Scheme 3a) with four C_{ipso}–Li interactions. As a plausible reaction pathway, the addition of PhMgBr onto complexes $[Mes_{3-n}Ph_nFe^{II}]^-$ affording quaternized $[Mes_{3-n}Ph_{n+1}Fe^{II}MgBr(THF)]^-$ intermediates was investigated by DFT calculations, and the results are discussed thereafter.

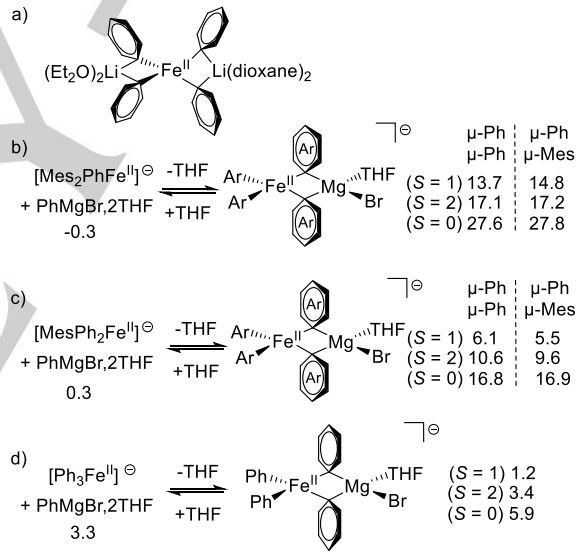

Scheme 3. a) Example of a structurally characterized quaternized tetraaryl-Fe^{II} species; DFT-computed energies for the quaternized $[Ar_2Fe(\mu\text{-}Ar)(\mu\text{-}Ar)MgBr(THF)]^-$ generated by the addition of PhMgBr on b) $[Mes_2PhFe^{II}]^-$, c) $[MesPh_2Fe^{II}]^-$ and d) $[Ph_3Fe^{II}]^-$. Computed energies (kcal.mol^{-1}) referenced to $[Mes_3Fe^{II}]^-$, similarly to Scheme 2. Ar = Mes or Ph.

Two types of quaternized species may be formed depending of the bridging ligands, either two phenyl rings or one phenyl and one mesityl rings. Only the latter can act as a reaction intermediate for the substitution of Mes by Ph in $[Mes_{3-n}Ph_nFe^{II}]^-$ (n = 0–2). Because bis-μ-Ph quaternized species can be involved in the formation of Fe^0 (*vide infra*), DFT-calculations of these analogous species are included in this section.

In the optimization of the structures of the quaternized adducts $[Mes_{3-n}Ph_{n+1}Fe^{II}MgBr(THF)]^-$, two interactions between a Mg^{II} cation and ipso-carbons, one from the phenyl anion brought by

PhMgBr and one from an aryl ligand of $[Mes_{3-n}Ph_nFe^{II}]^-$, have been envisioned, inspired by the structures of the reported lithium analogues (Scheme 3a). Because the local geometry around the iron center strongly differs between the starting tricoordinated *ate* species (planar, high-spin, S = 2, Scheme 2) and the quaternized adducts (distorted tetrahedron), one can expect a noticeable evolution of the ligand field during the process. Therefore, the structure of the quaternized adducts was optimized in the high-spin (S = 2, quintet), intermediate-spin (S = 1, triplet) and low-spin (S = 0, singlet) states. No stable adduct could be found starting from $[Mes_3Fe^{II}]^-$, most likely due to the steric pressure brought by the methyl groups in the *ortho* positions to the coordinated C-atom. This suggests that substitution in $[Mes_3Fe^{II}]^-$ doesn't proceed *via* an associative mechanism. It may be a concerted process or a dissociative one. However, it should be noticed that neither $[Mes_2Fe^{II}(THF)]$ nor $[Mes_4Fe^{II}_2]$ were detected, suggesting that if dissociation of $[Mes_3Fe^{II}]_-$ indeed occurs, the generated intermediate does not accumulate in solution.

Energies of the quaternized μ-Mes-μ-Ph species are reported in Scheme 3b and 3c (left columns). Whatever the S-value of the resulting intermediate, the difference in energy with those of the reactants decreases by approximatively 10 kcal.mol^{-1} upon increasing the n-value from 1 to 2. Consequently, generation of quaternized species is even more favored that the number of phenyl ligands in the starting triaryl-Fe^{II} complex is large. These calculated energy gaps are more important for the quaternized species in the S = 0 spin state, suggesting these (μ-Mes)(μ-Ph) intermediate species are generated in the S = 1 or S = 2 spin state. However, due to the proximity of both triplet and quintet DFT-computed energies, an accurate assessment of the ground spin state of these adducts cannot be reasonably performed. One important difference between these two electronic states relies on the geometry of the Fe^{II} ion. In the triplet optimized structures, the Fe^{II} ions accommodate an intermediate geometry, in-between the pseudo-tetrahedron and the planar square, whereas a local distorted tetrahedral geometry is observed for the quintet structures. This tendency is also in line with results reported for bis-mesitylated Fe^{II}-bisphosphine complexes, which proved to accommodate similarly either a quintet or a triplet ground spin state depending on their geometry.[11] The 15.1 and 5.2 kcal.mol^{-1} energy gaps calculated here for the formation of the S = 1 (μ-Mes)(μ-Ph) adducts starting from $[Mes_2PhFe^{II}]^-$ and $[MesPh_2Fe^{II}]^-$, respectively, are modest, suggesting that the corresponding energy barriers are accordingly also modest, in agreement with equilibrated ligand exchange reactions.

The same remarks apply to the quaternized adducts presenting two phenyl rings interacting with the Fe and Mg ions (see Scheme 3b and 3c, right column). In addition, they present energies similar of those of the (μ-Mes)(μ-Ph) species, suggesting that the energy costs for their formation is not an obstacle, especially if they evolve along a highly exothermic pathway. It should be noticed that the quaternized species formed from $[Ph_3Fe^{II}]^-$, namely $[Ph_2Fe(\mu\text{-}Ph)_2MgBr(THF)]^-$, is even more favored than the corresponding adducts investigated for n = 1 and n = 2. This intermediate is found to be only 0.1 kcal.mol^{-1} higher than the starting complex when generated in the S = 2 state, and even thermally favored, with an exothermicity of 2.1 kcal.mol^{-1} if generated in the S = 1 state (Scheme 3d). Overall, the thermal stability of these quaternized adducts is closely related to the steric pressure of the aryl ligands. Indeed, for each computed spin multiplicity, the higher the Mes:Ph ratio, the less stable the corresponding adduct with respect to the starting ate-complex. In the following sections, we examined the possibility of connecting the quaternized adducts formed from these complexes to Fe^0 and Fe^I oxidation states.

Reactivity of the quaternized Fe^{II} species

Apart from their role in the Mes/Ph exchange evidenced earlier (Scheme 2), a possible evolution pathway for the quaternized species discussed in the previous section would be the formation of a biaryl molecule, leading to the reduction of the iron ion to the Fe^0 oxidation state. A model surface for the formation of a biaryl molecule from a quaternized *ate*-Fe^{II} complex was computed, with all the three possible spin states for the Fe$^{0/II}$ couple (S = 2, quintet; S = 1, triplet; S = 0, singlet). $[Ph_3Fe^{II}]^-$ was taken as a model *ate* complex for this computational analysis. As outlined in Scheme 3d, quaternization of $^5[Ph_3Fe^{II}]^-$ leading to $[Ph_4Fe^{II}MgBr(THF)]^-$ is thermally feasible and the latter can reasonably be obtained in either a triplet (S = 1) or a quintet (S = 2) state. It can be noted that a quaternization step which would require an evolution of the iron spin state can occur thanks to an intersystem crossing (ISC).[21] As it can be expected from the evolution of the local environment at the metal (tricoordinated in $[Ph_3Fe^{II}]^-$ and tetracoordinated in $[Ph_4Fe^{II}MgBr(THF)]^-$), the ligand field decreases during the quaternization, narrowing the gap between the spin states from 11.3 to 4.7 kcal.mol^{-1} (Scheme 4).

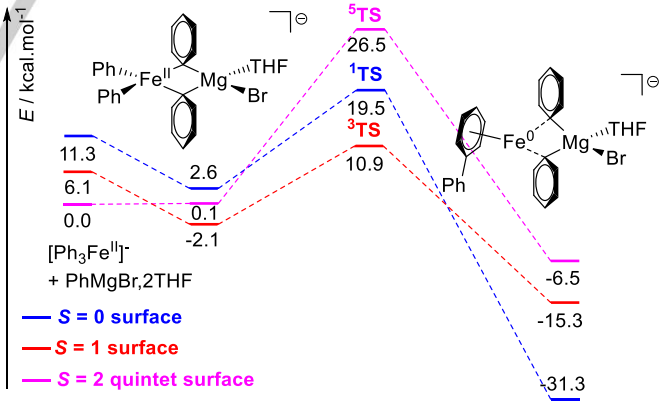

Scheme 4. DFT-computed surfaces (singlet state in blue; triplet state in red; quintet state in pink) for the quaternization of $[Ph_3Fe^{II}]^-$ followed by formation of a biphenyl molecule and 2-electron reduction of the iron center. Computed energies (kcal.mol^{-1}) referenced to $^5[Ph_3Fe^{II}]^-$.

Starting from a quaternized intermediate $[Ph_4Fe^{II}MgBr(THF)]^-$, a transition state which is likely to accommodate a triplet spin state can be reached (**^{3}TS**, computed activation barriers: 13.0 kcal.mol^{-1} from $^3[Ph_4Fe^{II}MgBr(THF)]^-$, 10.8 kcal.mol^{-1} from $^5[Ph_4Fe^{II}MgBr(THF)]^-$) and lead to the formation of the C–C bond and the concomitant 2-electron reduction of the Fe^{II} ion. The final

diamagnetic Fe^0 species $^1[(\eta^6\text{-PhPh})Fe^0Ph_2MgBr(THF)]^-$ is obtained in an overall exothermic step (ΔE = -31.3 kcal.mol^{-1} with respect to the starting $^5[Ph_3Fe^{II}]^-$ species). The possible existence of a transition state with an intermediate S = 1 spin can moreover explain the evolution of the iron spin state in the course of this reaction (S = 2 in the starting Fe^{II} complex, S = 0 in the final Fe^0 species). From $^1[(\eta^6\text{-PhPh})Fe^0Ph_2MgBr(THF)]^-$, a formal equivalent of Ph_2Mg can be released in the bulk, as well as a diamagnetic $(\eta^6\text{-PhPh})Fe^0$ fragment. The latter is highly unsaturated since it involves a 14-electron metal center. Its evolution towards more complex Fe^0-containing structures is in line with the detection of the Fe^0 oxidation state by Mössbauer spectroscopy. It is difficult to assign an accurate structure for the Fe^0 species evidenced by the Mössbauer experiments discussed in previous section since such species tend to quickly undergo aggregation processes. However, it can be noted that the nuclear parameters of the species II detected herein (Figure 3b) are close to those of molecular neutral Fe^0 complexes already reported, vide infra. The biphenyl molecule originally ligated to the Fe^0 center in $^1[(\eta^6\text{-PhPh})Fe^0Ph_2MgBr(THF)]^-$ is then detected by GC-MS, after destruction of the latter complex by acidic quench of the solution.

Similar sequences involving the quaternization of the Fe^{II} ion followed by the formation of a biaryl molecule and the 2-electron reduction of the iron site can also be undergone by $[Mes_2PhFe^{II}]^-$ and $[MesPh_2Fe^{II}]^-$ complexes (see Scheme 3b-c). Both species can lead to bis-μ-Ph and mixed (μ-Mes)(μ-Ph) quaternized species with energies of the S = 1 and S = 2 states distributed within less than 5.1 kcal.mol^{-1} starting from the same $[Ar_3Fe^{II}]^-$ complex, suggesting that the two quaternized adducts can interconvert. Assuming a similar pathway to that described in Scheme 4 for $[Ph_4Fe^{II}MgBr(THF)]^-$, the biaryl molecule is generated from the two terminal aryl ligands on the Fe^{II} site. We may reasonably assume that this step is exothermic, generating diamagnetic Fe^0 species. Accordingly, Mes–Mes and Mes–Ph are expected from the $[Mes_2PhFe^{II}]^-$ complex and PhMgBr whereas Mes–Ph and Ph–Ph can be formed from $[MesPh_2Fe^{II}]^-$. Because of the two methyl groups in ortho-positions to the carbon atom involved in the new C–C bond, formation of the less hindered biaryl molecule would be the less demanding process. Namely, Mes–Ph (resp. Ph–Ph) is favored versus Mes–Mes (resp. Mes–Ph). Indeed, this is fully in agreement with the decrease (resp. increase) of the amount of Mes–Mes (resp. Ph–Ph) biaryl molecule detected by GC-MS upon increasing addition of PhMgBr on $[Mes_3Fe^{II}]^-$ (see Figure 2c). The generation of quaternized species and their evolution with formation of a C–C bond between two terminal aryl ligands are sustained by experimental data from GC-MS and Mössbauer spectroscopy.

It must also be noted that the barrier leading to the reduction of the iron from $[Ph_3Fe^{II}]^-$ into $[(\eta^6\text{-PhPh})Fe^0Ph]^-$ proved to be greater than that of quaternized adducts discussed in this section (at least 16.0 kcal.mol^{-1} depending on the spin multiplicity, see Figure S9). Quaternization of $[Ph_3Fe^{II}]^-$ into $[Ph_4Fe^{II}MgBr(THF)]^-$, made possible in the presence of an excess of PhMgBr, thus allows to reduce the iron 2-electron reduction barrier for the sterically less hindered $[Ph_3Fe^{II}]^-$. In the case of the mixed Mes/Ph *ate* species, one could expect a competition between the two reductive eliminations (starting from either tri-coordinated species or from quaternized adducts). It is noteworthy that the progressive substitution of mesityl ligands of $[Mes_3Fe^{II}]^-$ by phenyls favors evolution towards the reduction at the Fe^0 stage from both steric and electronic points of view. First, the quaternization of ate-Fe^{II} intemediates as well as the formation of a biaryl molecule are more easily performed for low Mes:Ph ratios. Additionally, the gap between the spin multiplicities of the quaternized adducts is also narrowed for low Mes:Ph ratios (ranking between 4.7 kcal.mol^{-1} for $[Ph_4Fe^{II}MgBr(THF)]^-$ and 13.9 kcal.mol^{-1} for $[Mes_2Ph_2Fe^{II}MgBr(THF)]^-$, Scheme 3), which allows the step-bystep evolution of the system towards the S = 1 ground state of the Fe^0 product.

However, these results do not explain the concomitant observation of increasing Fe^I quantities evidenced by EPR spectroscopy (Figures 3a and S3). Formation of this oxidation state was then investigated in the last section of this report.

Formation of the Fe^I oxidation state from *ate*-Fe^{II} species.

A first hypothesis which could explain the formation of Fe^I species from *ate* $[Mes_{3-n}Ph_nFe^{II}]^-$ intermediates is the homolytic cleavage of a Mes–Fe^{II} bond (resp. Ph–Fe^{II}), releasing the $[Mes_{2-n}Ph_nFe^I]^-$ complex (resp. $[Mes_{3-n}Ph_{n-1}Fe^I]^-$) and an organic radical $Mes^\bullet$ (resp. $Ph^\bullet$). Recombination of those radicals may contribute to the distribution of biaryl products (Mes–Mes, Mes–Ph, Ph–Ph) evidenced earlier (Figure 2c). No trace of low or high-spin Fe^I species is detected by EPR spectroscopy when $FeCl_2$ is treated by an excess of MesMgBr (see SI), whereas up to 15% of low-spin mononuclear Fe^I species are detected when $FeCl_2$ is treated by 30 equivalents PhMgBr.[7] Because it was demonstrated that $[Mes_3Fe^{II}]^-$ formed in the former case and that $[Ph_3Fe^{II}]^-$ can be generated in the latter one, at least at low temperatures, these EPR observations suggest that if the homolytic cleavage of a Ar–Fe^{II} bond occurs in $[Ar_3Fe^{II}]^-$ despite the expected inertia of such C_{sp2}–metal bond, it should be easier for Ar = Ph. Results of the DFT-computation of the bond dissociation energies (BDEs) of the Mes–Fe^{II} and Ph–Fe^{II} bonds in $[Mes_3Fe^{II}]^-$ and $[Ph_3Fe^{II}]^-$ are reported in Scheme 5. The values are large (44.9 and 55.8 kcal.mol^{-1} for Mes–Fe^{II} and Ph–Fe^{II}, respectively) and definitely too large to be overcome at room temperature.

Similarly, homolytic cleavage of a Ph–Fe^{II} bond in a quaternized adduct such as $[Ph_4Fe^{II}MgBr(THF)]^-$ is highly endergonic (at least 38.8 kcal.mol^{-1}, Scheme 5). It is of note that the reactivity of the C_{sp2}–Fe^{II} bond drastically differs from the C_{sp2}–Fe^{III} analogues, which easily undergo homolytic dissociation leading to organic radicals and Fe^{II} intermediates.[7] The calculations evidenced that generation of Fe^I should operate relying on another mechanism.

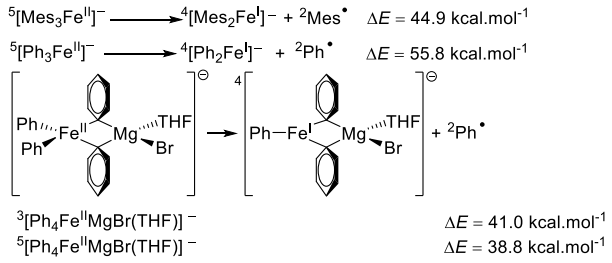

Scheme 5. DFT-computed bond dissociation energies for Ar─Fe^{II} bonds in various *ate*-Fe^{II} species (Ar = Mes, Ph); ground spin multiplicities superscripted.

Regarding the formation of Fe^{I} species from Fe^{II} sources, a second hypothesis which has been evoked by recent reports relies on the disproportionation of *ate* Fe^{II} polyhydrocarbyl intermediates, affording both Fe^{I} and Fe^{III} oxidation states. This has already been suggested independently by Bedford and Koszinowski, who respectively showed that $[(PhCH_2)_3Fe^{II}]^-$ and $[Ph_3Fe^{II}]^-$ species possibly underwent such redox events.[3,17] However, even if reduction of $FeCl_2$ by PhMgBr in THF:toluene mixtures led to the observation of both Fe^{I} and Fe^{III} species (EPR signals diagnostic of resp. S = 1/2 and S = 5/2 species being detected) we demonstrated in a previous report that these oxidation states were formed in unequal quantities according to EPR and Mössbauer speciations, and that the Fe^{III} oxidation state was observed in significantly smaller quantities than its Fe^{I} counterpart.[7] This is in contradiction with the hypothesis of a disproportionation, since one would expect the formation of equal quantities of Fe^{I} and Fe^{III} oxidation states. Similar results are observed upon EPR monitoring of the reaction of $[Mes_3Fe^{II}]^-$ with an excess of PhMgBr (Figure S5): under these conditions, the Fe^{I} oxidation state is obtained in higher quantities than Fe^{III}. This demonstrates that a disproportionation of *ate* $[Mes_{3-n}Ph_nFe^{II}]^-$ species, albeit feasible to a certain extent, cannot account for the formation of all the Fe^{I} quantity.[22]

The formation of Fe^{I} complexes from *ate* Fe^{II} intermediates is therefore difficult to explain if one considers typical reactivities of mononuclear organoiron(II) species such as homolytic cleavage of C_{sp2}─Fe^{II} bonds or disproportionation. On the other hand, it has recently been reported that polynuclear *ate*-Fe^{II} species could be formed by transmetallation of Grignard reagents with iron precursors. In particular, the dinuclear complex $[\{Fe^{II}(Ph)_2\}_2(\mu\text{-}Ph)_2]^{2-}$ was structurally characterized by X-Ray diffraction.[9] Magnetic circular dichroism (MCD), EPR and Mössbauer analyses showed that this dinuclear species involved two antiferromagnetically-coupled high-spin Fe^{II} ions. $[\{Fe^{II}(Ph)_2\}_2(\mu\text{-}Ph)_2]^{2-}$ is formed by reaction of a slight excess (4 equiv.) of PhMgBr with iron salts at low temperatures (T < –30°C when only $Fe(acac)_3$ and PhMgBr are introduced in THF, see ref 9). This complex moreover proved to be thermally unstable and to decompose upon warming above –30°C. Because such dinuclear species can formally be viewed as a dimeric form of the *ate* species $[Ph_3Fe^{II}]^-$, we sought to investigate the feasibility of forming the Fe^{I} oxidation state by a bimetallic reductive elimination step occurring in dinuclear complexes $[\{Fe^{II}(Mes;Ph)_2\}_2(\mu\text{-}Mes;Ph)_2]^{2-}$. The first step is the formation of a C–C bond between two aryl ligands that concomitantly leads to a formal decrease of the oxidation state of the two metal centers by one unit (from Fe^{II} to Fe^{I} herein, see Scheme 6a) within the dinuclear structure. The second step is the release of mononuclear Fe^{I} species detected by EPR spectroscopy.

We hypothesized that such dinuclear Fe^{II} species would result from the condensation of two identical or different mononuclear $[Mes_{3-n}Ph_nFe^{II}]^-$ complexes evidenced in this work. Because such a dimerization process has not been demonstrated for $[Ph_3Fe^{II}]^-$, we anticipate that these reactions are not favored and strongly displaced toward the mononuclear complexes. Accordingly, the energies of a series of selected symmetric dinuclear $[\{Fe^{II}(Mes;Ph)_2\}_2(\mu\text{-}Mes;Ph)_2]^{2-}$ species have been computed by DFT (Scheme 6b and SI). In order to mirror the electronic structure of the $[\{Fe^{II}(Ph)_2\}_2(\mu\text{-}Ph)_2]^{2-}$ complex, the Fe^{II} ions were described with high-spin configurations (S = 2) and we used a broken-symmetry (BS) approach to reproduce at best the diamagnetic ground state resulting from the antiferromagnetic exchange interaction between the two high-spin Fe^{II} ions. No dimeric structure could be characterized for $[Mes_3Fe^{II}]^-$, attesting to a too great steric pressure brought by the methyl groups in ortho positions to the coordinated C-atoms. The $[Mes_4Ph_2Fe^{II}{}_2]^{2-}$ complexes are located more than 50 kcal.mol^{-1} higher than the associated $[Mes_2PhFe^{II}]^-$ monomer (57.1 kcal.mol^{-1} for the μ-Mes;μ-Mes isomer, 52.2 kcal.mol^{-1} for the μ-Ph;μ-Ph analogue). Analogously, more than 30 kcal.mol^{-1} are determined for $[Mes_2Ph_4Fe^{II}{}_2]^{2-}$ complexes versus $[MesPh_2Fe^{II}]^-$ (33.5 kcal.mol^{-1} for the μ-Mes;μ-Mes isomer, 33.8 kcal.mol^{-1} for the μ-Ph;μ-Ph analogue). The smaller separation, still positive (9.4 kcal.mol^{-1}), is obtained for $[Ph_3Fe^{II}]_2{}^{2-}$ vs $[Ph_3Fe^{II}]^-$. The computed structure obtained for $[\{Fe^{II}(Ph)_2\}_2(\mu\text{-}Ph)_2]^{2-}$ is in good agreement with the geometrical parameters reported with $[Mg(acac)(THF)_4]_2{}^{2+}$ as a counter ion ($d_{Fe\text{-}Fe,calc}$ = 2.50 Å (exp: 2.52 Å), av. $d_{Fe\text{-}Ph,terminal,calc}$ = 2.09 Å (exp: 2.08 Å), av. $d_{Fe\text{-}\mu Ph,calc}$ = 2.20 Å (exp: 2.19 Å)).[9] It should be noticed that the large energy values calculated here corroborate the anticipated preference for monomeric forms.

Because the all-phenyl species $[\{Fe^{II}(Ph)_2\}_2(\mu\text{-}Ph)_2]^{2-}$ has the lowest formation energy among the investigated dimers, the feasibility of the formation of a C–C bond between the two bridging phenyls leading to the 1-electron reduction of the two iron sites was investigated starting from the computed structure.

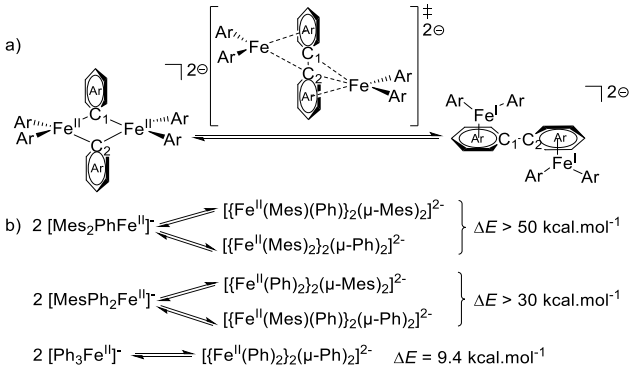

Scheme 6. a) First step of the bimetallic reductive elimination reaction connecting $[\{Fe^{II}(Ar)_2\}_2(\mu\text{-}Ar)_2]^{2-}$ and $[(\mu\text{-}ArAr)\{[Ar_2Fe^{I}]\}_2]^{2-}$ (Ar = Mes, Ph); b) computed energies for a selection of dimers (see SI for the structural and electronic details of each computed structure).

As described in Scheme 6a, the formation of the C–C bond leads to the dinuclear Fe^{I} complex $[\{[Ph_2Fe^{I}]\}_2(\mu\text{-PhPh})]^{2-}$ (denoted as $[Fe^{I}Fe^{I}]$) which formally involves two $[Fe^{I}(Ph)_2]^{-}$ moieties and a bridging PhPh molecule. Owing to the antiferromagnetic coupling of the two Fe^{II} ions in $[\{Fe^{II}(Ph)_2\}_2(\mu\text{-}Ph)_2]^{2-}$ (denoted as $[Fe^{II}Fe^{II}]$), a broken-symmetry approach was used to investigate the starting $[Fe^{II}Fe^{II}]$ and the resulting $[Fe^{I}Fe^{I}]$ species. Two energetically close broken-symmetry states could be located for $[Fe^{II}Fe^{II}]$. The most stable one, $[(^5Fe^{II})(^5Fe^{II})]$, involves two high-spin Fe^{II} ions, accordingly to the experimentally characterized ground state of $[\{Fe^{II}(Ph)_2\}_2(\mu\text{-}Ph)_2]^{2-}$ (Table 2, Entry 1). Lying 4.5 kcal.mol^{-1} above the latter, the second state which has been located involves two Fe^{II} ions in a triplet configuration ($[(^3Fe^{II})(^3Fe^{II})]$, Table 2, Entry 2). In that latter structure, the Fe^{II} ions accommodate an intermediate geometry (in-between tetrahedral and square-planar environments).

Entry	Species	Iron site properties		ΔE
		Local electronic spin value (S_{Fe})	Calculated (ρ_{Fe1} ; ρ_{Fe2})	
1	$[\{Fe^{II}(Ph)_2\}_2(\mu\text{-}Ph)_2]^{2-}$	2	+3.4 ; -3.4	9.4
2		1	+2.6 ; -2.5	13.9
3	$[\{[Ph_2Fe^{I}]\}_2(\mu\text{-PhPh})]^{2-}$	3/2	+2.8 ; -3.0	-9.0
4		1/2	+1.5 ; -1.5	-49.3

Table 2. DFT-computed electronic formation energies (ΔE (kcal.mol^{-1}); with respect to 2 equiv. $^5[Ph_3Fe^{II}]^{-}$) and spin density at the iron ρ_{Fe} for dimeric species $[\{Fe^{II}(Ph)_2\}_2(\mu\text{-}Ph)_2]^{2-}$ and $[\{[Ph_2Fe^{I}]\}_2(\mu\text{-PhPh})]^{2-}$ (broken-symmetry approach).

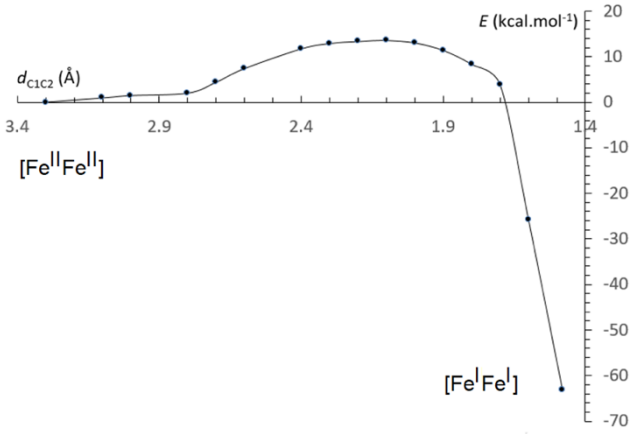

Figure 4. DFT-computed potential energy surface (PES) scan for the formation of a biphenyl molecule with reduction of the Fe^{II} ions to the Fe^{I} oxidation state, connecting $[(^3Fe^{II})(^3Fe^{II})]$ and $[(^2Fe^{I})(^2Fe^{I})]$ (computed electronic energies, broken-symmetry surface; no PCM solvation model was added).

Following a bimetallic reductive elimination path on the broken-symmetry surface, $[(^5Fe^{II})(^5Fe^{II})]$ will afford complex $[(^4Fe^{I})(^4Fe^{I})]$ with two high-spin Fe^{I} ions (Table 2, Entry 3) whereas $[(^3Fe^{II})(^3Fe^{II})]$ can afford the $[(^2Fe^{I})(^2Fe^{I})]$ species with low-spin Fe^{I} ions (Table 2, Entry 4).[23] The reduced dinuclear complex $[\{[Ph_2Fe^{I}]\}_2(\mu\text{-PhPh})]^{2-}$ was found to be unquestionably more stable than $[\{Fe^{II}(Ph)_2\}_2(\mu\text{-}Ph)_2]^{2-}$, regardless of the considered spin multiplicities. Stability of $[\{[Ph_2Fe^{I}]\}_2(\mu\text{-PhPh})]^{2-}$ was maximized with two Fe^{I} centers accommodating a low-spin multiplicity ($S_1 = S_2 = 1/2$, stabilization of 49.3 kcal.mol^{-1} with respect to the reactants, Table 2, entry 4).[24] It is also noticeable that a significant delocalization of the spin density occurs on the four Fe-ligated C atoms in $[Fe^{I}Fe^{I}]$ (Entries 3-4), in agreement with what we reported for similar dicoordinated Fe^{I} *ate* species.[24] These results in hand, a relaxed scan of the potential energy surface (PES) of the formation of the biphenyl molecule has been performed using a broken-symmetry approach, the distance between the two bridging carbon atoms C_1 and C_2 being considered as the reaction coordinate. Owing to the greater stability of the Fe^{I} ions in a low-spin configuration at the end of the process, the pathway connecting $[(^3Fe^{II})(^3Fe^{II})]$ and $[(^2Fe^{I})(^2Fe^{I})]$ has been considered, as reproduced in Figure 4. The required barrier can be evaluated at ca. 13.6 kcal.mol^{-1} with respect to the starting $[^3(Fe^{II})^3(Fe^{II})]$ dimer.

Generation of bis-Fe^{I} species due to the formation of biphenyl molecules presents a large driving force with respect to the starting mononuclear high-spin $[Ph_3Fe^{II}]^{-}$ complex (Scheme 7a). DFT-calculations favor a process where the Fe^{I} ions present a low-spin state. This is fairly in line with the EPR data. However, at this stage, the Fe^{I} ions are in a dinuclear structure whereas only isolated monomeric Fe^{I} species can give the detected EPR signal. A last step is thus required to fully explain the EPR data. The complex $[(\eta^6\text{-PhPh})Fe^{I}(Ph)_2]^{-}$ has been previously X-ray characterized[8] and its released form $[(^2Fe^{I})(^2Fe^{I})]$ would also generate the mononuclear $[Ph_2Fe^{I}]^{-}$ fragment. The latter can be stabilized by the toluene used as a cosolvent with THF in the EPR experiments. Indeed, DFT-calculations show that formation of two $[(\eta^6\text{-}C_6H_5Me)Fe^{I}(Ph)_2]^{-}$ complexes from $[(^2Fe^{I})(^2Fe^{I})]$, with the release of one biphenyl molecule, is exothermic (–6.9 kcal.mol^{-1}, see Scheme 7b).

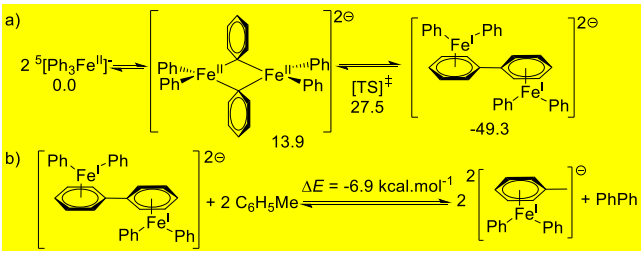

Scheme 7. a) Overall DFT-computed surface for the formation of $[(^2Fe^{I})(^2Fe^{I})]$ from $^5[Ph_3Fe^{II}]^{-}$, via $[(^3Fe^{II})(^3Fe^{II})]$ (dinuclear species computed using a broken-symmetry approach); b) evolution of $[(^2Fe^{I})(^2Fe^{I})]$ towards mononuclear $[(\eta^6\text{-}C_6H_5Me)Fe^{I}(Ph)_2]^{-}$ in toluene.

Thanks to the formation of the dimeric adduct $[\{Fe^{II}(Ph)_2\}_2(\mu\text{-}Ph)_2]^{2-}$ which then undergoes a bimetallic reductive elimination, $[Ph_3Fe^{II}]^{-}$ is the only *ate*-Fe^{II} species amongst the $[Mes_3$-

$_n$Ph$_n$Fe^{II}]$^-$ complexes able to afford the Fe^I oxidation state evidenced by EPR (Figure 3a and Scheme 7). This reaction process is in agreement with the formation of Fe^I by reduction of [Mes$_3$Fe^{II}]$^-$ observed only for high PhMgBr:[Mes$_3$Fe^{II}]$^-$ ratios. Progressive addition of PhMgBr on [Mes$_3$Fe^{II}]$^-$ leads to the substitution of an increasing number of mesityl ligands by phenyls. Because of the methyl groups in ortho-positions, the presence of mesityl ligands seems to preclude the mononuclear species from generating bis-Fe^{II} complexes. DFT studies strongly suggest that such a dimerization process can only apply to [Ph$_3$Fe^{II}]$^-$, that is the fully substituted complex.

Overall mechanistic picture

A progressive substitution of the mesityl groups in [Mes$_3$Fe^{II}]$^-$ by phenyl anions upon addition of PhMgBr leads to the formation of increasing quantities of [Mes$_{3-n}$Ph$_n$Fe^{II}]$^-$ species (n = 1-3). In the presence of PhMgBr, a quaternization of the Fe^{II} ion can occur, leading to [Mes$_{3-n}$Ph$_{n+1}$Fe^{II}MgBr(THF)]$^-$ (n = 1-3) intermediates. Starting from those quaternized adducts, a bielectronic reductive elimination affords Fe^0 oxidation state (as evidenced by Mössbauer spectroscopy) and organic biaryls Mes─Mes, Mes─Ph and Ph─Ph (as evidenced by GC-MS). For high PhMgBr:[Mes$_3$Fe^{II}]$^-$ ratios, once all the mesityl groups in [Mes$_3$Fe^{II}]$^-$ have been displaced by phenyl anions, a second pathway, energetically much more demanding, can be followed. [Ph$_3$Fe^{II}]$^-$ can indeed lead to the formation of the dinuclear complex [{Fe^{II}(Ph)$_2$}$_2$(μ-Ph)$_2$]$^{2-}$, which then leads to Fe^I oxidation state after an intramolecular bimetallic reductive elimination.

Scheme 8 summarizes these different evolution pathways. The respective values of the computed energies required for the formation of the Fe^I and Fe^0 oxidation states (resp. 27.5 kcal.mol^{-1}, Scheme 7a, and 10.8 or 13.0 kcal.mol^{-1}, Scheme 4) also explain why the latter is formed in much higher quantities, as evidenced in the first section of this article by Mössbauer and EPR spectroscopies.[25]

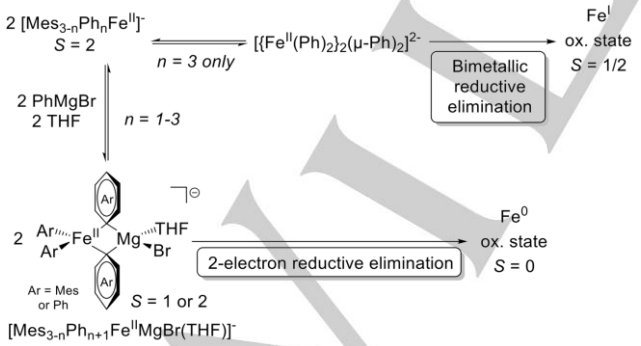

Scheme 8. summary of the possible evolution pathways connecting [Ph$_3$Fe^{II}]$^-$ to the Fe^0 and Fe^I oxidation states.

Conclusions

We demonstrated that *ate*-Fe^{II} species [Mes$_{3-n}$Ph$_n$Fe^{II}]$^-$ (n = 1-3) with a low steric pressure at the metal, obtained by progressively substituting the mesityl ligands of the kinetically stable [Mes$_3$Fe^{II}]$^-$ by phenyl anions, are key intermediates on the formation route to the Fe^0 and Fe^I oxidation states usually observed in the course of the reduction of iron salts with Grignard reagents. In the presence of PhMgBr, a plausible evolution pathway of the *ate*-Fe^{II} species [Mes$_{3-n}$Ph$_n$Fe^{II}]$^-$ is the quaternization of the Fe^{II} ions affording [Mes$_{3-n}$Ph$_{n+1}$Fe^{II}MgBr(THF)]$^-$ (n = 1-3), which lead to the formation of Fe^0 oxidation state by 2-electron reductive elimination. This mechanism involves two successive intersystem crossings, and overall connects high-spin [Ar$_3$Fe^{II}]$^-$ species with diamagnetic Fe^0 complexes.

The tris-phenylated species [Ph$_3$Fe^{II}]$^-$, formed by substituting all the mesityl ligands of [Mes$_3$Fe^{II}]$^-$ by phenyl anions, can also afford the dinuclear complex [{Fe^{II}(Ph)$_2$}$_2$(μ-Ph)$_2$]$^{2-}$ by dimerization, albeit in an energetically demanding pathway. This dimeric intermediate leads to the formation of Fe^I oxidation state by a bimetallic reductive elimination. This dimerization being hampered for *ate* [Mes$_{3-n}$Ph$_n$Fe^{II}]$^-$ intermediates involving one or more bulky aryl groups (Ar = Mes), this explains why Fe^I oxidation state is not detected when sterically hindered Grignard reagents are used as nucleophiles in these systems.

In both Fe^0 and Fe^I formation mechanisms, steric pressure and spin crossovers occurring along these pathways proved to be the determinant parameters.

In the context of Fe-catalyzed cross-coupling chemistry, the Fe^0 and Fe^I oxidation states formed by evolution of *ate*-Fe^{II} species are either on-cycle active species, or off-cycle intermediates which are detrimental to the efficiency of the catalytic system. These mechanistic findings can thus give new guidelines for the design of finely tailored ligands in iron-mediated C─C bond formation strategies, opening up the possibility to selectively obtain a sole iron oxidation state upon the precatalyst reduction.

Experimental Section

All calculations were carried out using the Gaussian09 v. D.01 code. Theory level: OPBE / def2TZVPP (Fe) / 6-31+G* (C, H, Mg, O) / 6-311G (Br), PCM-THF, unless specified otherwise. See SI for the corresponding references.

X-band EPR spectra were recorded on a Bruker ELEXSYS 500 spectrometer equipped with a Bruker ER 4116DM X band resonator, an Oxford Instrument continuous flow ESR 900 cryostat, and an Oxford ITC 503 temperature control system.

Mössbauer spectra were recorded on a strong-field Mössbauer spectrometer equipped with an Oxford Instruments Spectromag 4000 cryostat containing an 8 T split-pair superconducting magnet. The spectrometer was operated in a constant-acceleration mode in transmission geometry. The isomer shifts are referenced against that of a metallic iron foil at room temperature. Analysis of the data was performed with the program WMOSS (WMOSS4 Mössbauer Spectral Analysis Software, www.wmosss.org, 2009−2015) and a homemade program.[26] Simulation of Mössbauer parameters by DFT calculations

were performed using the ORCA v. 3.0.3 code at the BP86-D3BJ - TZVP / CP(PPP) (Fe) level (see SI for the corresponding references).

Acknowledgements

G.L. thanks the ANR for its financial support (project JCJC-SIROCCO, 2016-2020). Dr Eric Brémond (ITODYS, Univ. Paris-Diderot) is thanked for fruitful discussions. Gabriel Durin (UMR 3685, CEA Saclay) is thanked for technical assistance. G. B. and M. C. thank the Labex ARCANE (grant ANR-11-LABX-0003-01) and the Labex CBH-EUR-GS (grant ANR-17-EURE-0003) for their financial supports.

Keywords: iron hydrocarbyls • reduction • Mössbauer spectroscopy • EPR spectroscopy • DFT calculations

[1] a) M. Tamura, J. K. Kochi, *J. Am. Chem. Soc.* **1971**, *93*, 1487-1489; b) S. M. Neumann, J. K. Kochi, *J. Org. Chem.* **1975**, *40*, 599-606; c) G. Cahiez, H. Avedissian, *Synthesis* **1998**, *1998*, 1199-1205; d) B. D. Sherry, A. Fürstner, *Acc. Chem. Res.* **2008**, *41*, 1500-1511, and references cited; e) R. B. Bedford, *Acc. Chem. Res.* **2015**, *48*, 1485-1493; f) I. Bauer, H.-J. Knölker, *Chem. Rev.*, **2015**, *115*, 3170-3387; g) S. B. Muñoz III, S. L. Daifuku, W. W. Brennessel, M. L. Neidig, *J. Am. Chem. Soc.* **2016**, *138*, 7492-7495; h) S. H. Carpenter, M. L. Neidig, *Isr. J. Chem.* **2017**, *57*, 1106-1116; i) J. D. Sears, P. G. N. Neate, M. L. Neidig, *J. Am. Chem. Soc.* **2018**, *140*, 11872-11883; j) M. L. Neidig, S. H. Carpenter, D. J. Curran, J. C. DeMuth, V. E. Fleischauer, T. E. Iannuzzi, P. G. N. Neate, J. D. Sears, N. J. Wolford *Acc. Chem. Res.* **2019**, *52*, 140-150.

[2] a) S. L. Daifuku, J. L. Kneebone, B. E. R. Snyder, M. L. Neidig, *J. Am. Chem. Soc.* **2015**, *137*, 11432-11444; b) J. L. Kneebone, W. W. Brennessel, M. L. Neidig, *J. Am. Chem. Soc.* **2017**, *139*, 6988-7003.

[3] R. B. Bedford, P. B. Brenner, E. Carter, P. M. Cogswell, M. F. Haddow, J. N. Harvey, D. M. Murphy, J. Nunn, C. H. Woodall, *Angew. Chem. Int. Ed.* **2014**, *53*, 1804-1808.

[4] V. E. Fleischauer, S. B. Muñoz III, P. G. N. Neate, W. W. Brennessel, M. L. Neidig, *Chem. Sci.* **2018**, *9*, 1878-1891.

[5] J. D. Sears, P. G. N. Neate, M. L. Neidig, *J. Am. Chem. Soc*. **2018**, *140*, 11872-11883.

[6] a) C. J. Adams, R. B. Bedford, E. Carter, N. J. Gower, M. F. Haddow, J. N. Harvey, M. Huwe, M. À. Cartes, S. M. Mansell, C. Mendoza, D. M. Murphy, E. C. Neeve, J. Nunn, *J. Am. Chem. Soc.* **2012**, *134*, 10333-10336; b) M. Guisán-Ceinos, F. Tato, E. Buñuel, P. Calle and D. J. Cárdenas, *Chem. Sci.* **2013**, *4*, 1098-1104; c) G. Lefèvre, A. Jutand, *Chem. Eur. J.* **2014**, *20*, 4796-4805.

[7] M. Clémancey, T. Cantat, G. Blondin, J.-M. Latour, P. Dorlet, G. Lefèvre, *Inorg. Chem.* **2017**, *56*, 3834-3848.

[8] F. E. Zhurkin, M. D. Woodrich, X. Hu, *Organometallics* **2017**, *36*, 499-501.

[9] S. H. Carpenter, T. M. Baker, S. B. Muñoz III, W. W. Brennessel, M. L. Neidig, *Chem. Sci.* **2018**, *9*, 7931-7939.

[10] S. L. Daifuku, M. H. Al-Afyouni, B. E. R. Snyder, J. L. Kneebone, M. L. Neidig, *J. Am. Chem. Soc.* **2014,** *136*, 9132-9143.

[11] E. J. Hawrelak, W. H. Bernskoetter, E. Lobkovsky, G. T. Yee, E. Bill, P. J. Chirik, *Inorg. Chem.* **2005**, *44*, 3103-3111.

[12] M. Irwin, R. K. Jenkins, M. S. Denning, T. Krämer, F. Grandjean, G. J. Long, R. Herchel, J. E. McGrady, J. M. Goicoechea, *Inorg. Chem.* **2010**, *49*, 6160-6171.

[13] H. Müller, W. Seidel, H. Görls, *J. Organomet. Chem.* **1993**, *445*, 133-136.

[14] C.-L. Sun, H. Krause, A. Fürstner, *Adv. Synth. Catal.* **2014**, *356*, 1281-1291.

[15] A. Klose, E. Solari, C. Floriani, A. Chiesi-Villa, C. Rizzoli, N. Re, *J. Am. Chem. Soc.* **1994**, *116*, 9123-9135.

[16] T. Parchomyk, S. Demeshko, F. Meyer, K. Koszinowski, *J. Am. Chem. Soc.* **2018**, *140*, 9709-9720.

[17] T. Parchomyk, K. Koszinowski, *Chem. Eur. J.* **2016**, *22*, 15609-15613.

[18] T. Parchomyk, S. Demeshko, F. Meyer, K. Koszinowski, *J. Am. Chem. Soc.* **2018,** *140*, 9709-9720.

[19] S. F. Parker, C. H. F. Peden, *J. Organomet. Chem.* **1984**, *272*, 411-416.

[20] a) T. A. Bazhenova, R. M. Lobkovskaya, R. P. Shibaeva, A. K. Shilova, M. Gruselle, G. Leny, E. Deschamps, E. *J. Organomet. Chem*. **1983**, *244*, 375-382; b) A. Fürstner, R. Martin, H. Krause, G. Seidel, R. Goddard, C. W. Lehmann, *J. Am. Chem. Soc.*, **2008**, *130*, 8773-8787.

[21] The importance of intersystem crossings in the transmetallation step between Grignard reagents and diimine Ni^{II} complexes has also been recently reported by Zimmerman *et al.* in the course of catalyst-transfer polymerization studies. See A. K. Vitek, A. K. Leone, A. J. McNeil, P. M. Zimmerman, *ACS Catal.* **2018**, *8*, 3655-3666. For a review on the influence of spin state on transition-metal complexes reactivity, see J. Harvey, R. Poli, *Coord. Chem. Rev.* **2003**, *238-239*, 347-361.

[22] This is in agreement with the respective energies computed for similar $[(\eta^6\text{-arene})Fe^{I}(Ph)_2]^-$ systems (arene = toluene or biphenyle), in which the low-spin isomer is favored by ca. 20 $kcal.mol^{-1}$ with respect to its high-spin analogue. See L. Rousseau, E. Brémond, G. Lefèvre, *New. J. Chem.* **2018**, *42*, 7612-7616.

[23] Formation of dimeric species $[\{Fe^{II}(Ph)_2\}_2(\mu\text{-}Ph)_2]^{2-}$ could also lead to Fe^0 oxidation state, by reductive elimination of a biphenyl molecule from two phenyl ligands in terminal positions. However, since the formation of the $[(Fe^{II})(Fe^{II})]$ adduct is much more demanding than formation of the quaternized species $[Ph_4Fe^{II}MgBr(THF)]^-$, the most important part of the Fe^0 oxidation state is likely to originate from evolution of the latter.

[24] a) C. Charavay, S. Segard, F. Edon, M. Clémancey, G. Blondin, *SimuMoss software*; CEA/DRF/BIG, CNRS, Université Grenoble Alpes, 2012; b) M. Carboni, M. Clémancey, F. Molton, J. Pécaut, C. Lebrun, L. Dubois, G. Blondin, J.-M. Latour, *Inorg. Chem.* **2012**, *51*, 10447−104

[25] Formation of dimeric species $[\{Fe^{II}(Ph)_2\}_2(\mu\text{-}Ph)_2]^{2-}$ could also lead to Fe^0 oxidation state, by reductive elimination of a biphenyl molecule from two phenyl ligands in terminal positions. However, since the formation of the $[(Fe^{II})(Fe^{II})]$ adduct is much more demanding than formation of the quaternized species $[Ph_2Fe^{II}(\mu\text{-}Ph)_2MgBr(THF)]^-$, the most important part of the Fe^0 oxidation state is likely to originate from evolution of the latter.

[26] a) C. Charavay, S. Segard, F. Edon, M. Clémancey, G. Blondin, SimuMoss software; CEA/DRF/BIG, CNRS, Université Grenoble Alpes, 2012; b) M. Carboni, M. Clémancey, F. Molton, J. Pécaut, C. Lebrun, L. Dubois, G. Blondin, J.-M. Latour, *Inorg. Chem.* **2012**, *51*, 10447−10460